Philosophical Magazine,
Vol. 85, No. 22, 1st August 2005, 2561–2580

Taylor & Francis
Taylor & Francis Group

Dislocation decoration and raft formation in irradiated materials

M. WEN†, N. M. GHONIEM*† and B. N. SINGH‡

†Department of Mechanical and Aerospace Engineering,
University of California, Los Angeles, CA 90095, USA
‡Materials Research Department, RISØ National Laboratory,
DK-4000 Roskilde, Denmark

(*Received 11 October 2004; in final form 23 February 2005*)

Experimental observations of dislocation decoration with self-interstitial atom (SIA) clusters and of SIA cluster rafts are analysed to establish the mechanisms controlling these phenomena in bcc metals. The elastic interaction between SIA clusters, and between clusters and dislocations is included in kinetic Monte Carlo (KMC) simulations of damage evolution in irradiated bcc metals. The results indicate that SIA clusters, which normally migrate by 1D glide, rotate due to their elastic interactions, and that this rotation is necessary to explain experimentally-observed dislocation decoration and raft formation in neutron-irradiated pure iron. The critical dose for raft formation in iron is shown to depend on the intrinsic glide/rotation characteristics of SIA clusters. The model is compared with experimental observations for the evolution of defect cluster densities (sessile SIA clusters and nano-voids), dislocation decoration characteristics and the conditions for raft formation.

1. Introduction and background

Primary defect clusters produced in displacement cascades play an important role in microstructure evolution and hence properties of irradiated materials. The formation of self-interstitial atom (SIA) and vacancy clusters within the cascade volume has been confirmed by both experiments and computer simulations. For example, diffuse X-ray scattering on fast neutron irradiated metals at temperatures below stage II provide evidence for spontaneous SIA cluster formation by cascades [1]. Molecular dynamics (MD) studies have shown that SIA clusters can be produced directly in high energy cascades, without the need for diffusion during the cool-down phase of cascades [2–6]. SIA clusters are directly produced on the periphery of neutron collision cascades and they may contain from a few atoms up to tens of atoms in the near vicinity of the cascade [2, 4]. The most stable configuration of SIA clusters for sizes larger than a few SIAs is found to be a set of ⟨111⟩ crowdions [7]. SIA clusters

*Corresponding author. Email: ghoniem@ucla.edu

Philosophical Magazine
ISSN 1478–6435 print/ISSN 1478–6443 online
http://www.tandf.co.uk/journals
DOI: 10.1080/14786430500154281

are highly glissile [5] and large SIA clusters in α-Fe can collapse to form perfect dislocation loops with the Burgers vector $a/2\langle 111\rangle$ and {110} habit plane. SIA clusters have been shown to execute one-dimensional (1D) random motion in their slip direction [8]. Small interstitial loops can further organize themselves to develop *patches* or *rafts* at elevated temperature [9], and dislocations are often observed being heavily decorated by SIA clusters in the form of small interstitial loops. Using the Foreman and Eshelby [10] formulation of the elastic interaction between prismatic dislocation loops, Barnes [11] discussed the migration of point defect clusters by slip, climb or both processes. A raft configuration of loops was suggested to result from loop–loop elastic interaction, where loops on neighbouring basal planes adjust their positions and orientations to take up an overall low energy configuration.

The formation of SIA loop rafts and the decoration of dislocations with SIA clusters have become important issues for understanding radiation hardening and embrittlement under cascade damage conditions. It has been experimentally observed that in the deformation process of metals and alloys under cascade damage conditions, an increase of the upper yield stress occurs as a result of radiation hardening, and is followed by an immediate yield drop and plastic instability [12]. The 'cascade induced source hardening' (CISH) model was proposed by Singh *et al.* [13] and applied to explain the occurrence of yield drop. In this model, a dislocation decorated with interstitial loops is assumed to be confined by the surrounding atmosphere of loops and unable to act as a dislocation source until the applied resolved stress reaches a critical de-trapping level. Huang and Ghoniem [14] investigated the interaction dynamics between sessile SIA clusters and dislocations using the method of parametric dislocation dynamics (PDD) simulations and found a smaller critical resolved shear stress (CRSS) compared to the results of Kroupa [15] and Trinkaus *et al.* [16] as a consequence of dislocation flexibility.

Loop rafts were first observed in graphite [11]. Possible mechanisms for raft formation and dislocation decoration by small loops were discussed by Brimhall and Mastel [9] as a result of their experimental observations of irradiated Mo. They attributed these phenomena to the mechanism of SIA cluster glide combined with self-climb. However, this mechanism was limited to higher temperatures, where both prismatic glide and conservative climb are operative. Eyre *et al.* [17] also concluded that the growth of interstitial loops during post-irradiation annealing occurs by combined glide and climb processes. Since these early observations, more recent experiments revealed raft formation in Mo, TZM (Mo–0.5Ti–0.1Zr), Cu and Fe [18–22]. The formation of SIA loop rafts in Mo was observed to occur at a relatively low dose of 5.4×10^{-3} dpa [21].

The segregation of the microstructure into rafts of loops and isolated loops eventually leads to a very heterogeneous microstructure at a dose of 0.72 dpa. Eldrup *et al.* [18] showed that the density of SIA clusters in both Fe and Cu first increases with dose. The formation of SIA cluster rafts is very efficient in bcc metals. The size and spatial distribution of rafts were found to be heavily dependent on material purity, irradiation temperature and dose. The size distribution may range from 10–100 nm [9]. In many microstructural studies of neutron irradiated metals and alloys, segregation of small SIA loops is often observed in the vicinity of dislocations in the form of a Cottrell-like atmosphere [23]. The phenomenon of

decoration of dislocations by small interstitial loops under cascade damage conditions has been observed in a wide range of metals and alloys [9, 21, 24].

Atomistic computer simulations can be very helpful in determining the physical mechanisms that explain such experimental observations. However, MD or *ab initio* simulations of the collective behaviour of SIA clusters in the presence of a stress field are currently not feasible because of the short times and small volume limits. Kinetic Monte Carlo (KMC) simulations, on the other hand, provide another alternative to perform atomic-level modelling of defect kinetics and microstructure evolution over significantly longer length and time scales [6, 25]. While it is recognized that elastic interactions between defects have significant effects on microstructure evolution and mechanical properties, the influence of internal strain fields on the long range migration and self-organization of defects has not yet been previously investigated with the KMC technique. In the present work, the KMC computer simulation method is further developed to incorporate the effects of internal strain fields. The main objective here is to show the strong influence of these interactions on the spatial inhomogeneity and segregation of point defects, which are manifest in dislocation decoration and the formation of rafts of SIA clusters. We compare model predictions with experimental observations on neutron irradiated iron to determine the main physical mechanisms responsible for dislocation decoration, raft formation and defect damage accumulation.

In section 2, we first introduce an elastic model for the interaction between point defect clusters. Using this model, we develop a KMC-based model for microstructure evolution, which explicitly includes stress field effects. The main features of the model are presented in section 3 and the model is applied to the experimental conditions of neutron-irradiated pure iron at $\simeq 70^{\circ}$C in the High Flux Irradiation Reactor (HFIR) at Oak Ridge National Laboratory [18]. Results of the model and comparison with experiments are described in section 4, while the summary and conclusions are finally given in section 5.

2. Elastic interaction of defects

Applications of linear elasticity theory to the study of defects and dislocations have been established for almost half a century (see e.g. [10, 15, 26, 27]). Nevertheless, modern computational techniques, such as the KMC method, has yet to take advantage of these early developments. In the present work, we are interested in point defect clusters of simple geometry (i.e. SIA loops or spherical vacancy clusters), where analytical elastic solutions are available for isotropic materials. We use here the analytical solutions developed by Kroupa [15] for circular prismatic dislocation loops to represent the elastic fields of SIA clusters. The numerical method developed by Ghoniem and Sun [28] and Ghoniem [29] is employed to evaluate the stress field of an arbitrary-shaped grown-in slip dislocation loop. We represent here SIA clusters as small prismatic, rigid and circular dislocation loops. The relationship between radius of the loop (R) and the number of defects (N) is $N = 2^{1/2}\pi R^2/a^2$. We approximate vacancy clusters produced in cascades as small spherical voids, with an effective radius of $r_v = (3N\Omega/4\pi)^{1/3}$, where Ω is the atomic volume and N the number of vacancies in the cluster.

The interaction energy of two dislocation loops over the volume V is expressed as

$$E_{\mathrm{I}} = \int_V \sigma_{ij}^{(1)} \varepsilon_{ij}^{(2)} \, \mathrm{d}V \tag{1}$$

in which $\sigma_{ij}^{(1)}$ is the stress arising from the first dislocation loop and $\varepsilon_{ij}^{(2)}$ is the strain originating in the other. If the second loop or defect cluster is assumed to be infinitesimal, the interaction energy can be simplified to [15]

$$E_{\mathrm{I}} = \delta A^{(2)} n_i^{(2)} \sigma_{ij}^{(1)} b_j^{(2)}, \tag{2}$$

where $n_i^{(2)}$ is the unit normal vector to the defect cluster habit plane of area $\delta A^{(2)}$. The interaction energy between an existing slip dislocation (grown-in) and an SIA cluster is obtained by substituting the expressions for σ_{ij} [14] into (2). The cluster is designated with the superscript (2) and the slip loop has a Burgers vector $b_n^{(1)}$. The stress tensor of a grown-in dislocation loop is assumed to be constant over the cross-section of the small SIA cluster. The same procedure is followed when the interaction energy between two SIA clusters is calculated, except that the stress field of one of them is determined analytically following [15]. Single point defects and small vacancy clusters are treated as centres of dilatation and the interaction energy simplifies to

$$E_{\mathrm{I}} = -\frac{4}{9} \pi r_0^3 \varepsilon_{ii}^{(2)} \sigma_{jj}^{(1)}, \tag{3}$$

where $\varepsilon_{ii}^{(2)}$ is the dilatation and r_0 is the effective radius of a point defect. The dilation, ε_{ii}, in this case, is given by $\varepsilon_{ii} = \mu \delta V / (\pi \kappa r_{\mathrm{v}}^3)$, where δV is the volume change and $3\kappa = 3\lambda + 2\mu$ is the bulk modulus with λ and μ being Lame's constants.

3. Computational model

3.1. *Methodology*

The jump frequency for a SIA cluster, i, is given by

$$r_i = \omega_0 \exp\left(-\frac{E_i}{k_{\mathrm{B}} T}\right), \tag{4}$$

where ω_0 is a pre-exponential factor of the defect cluster, k_{B} is the Boltzmann constant, E_i is the 'effective' activation energy and T is the absolute temperature. The total cluster activation energy for migration is then given by

$$E_i = E_{\mathrm{m}} + \Delta E_{\mathrm{int}}, \tag{5}$$

where E_{m} is the activation energy in a perfect crystal and ΔE_{int} is the difference in the interaction energy of a defect cluster placed at two neighbouring equivalent positions in the crystal.

Define $P(i) = r_i / \sum_{i=1}^{M} r_i$ as the probability distribution function (PDF) for cluster jumps. Then, the cumulative distribution function (CDF) is given by

$C(m) = \sum_{i=1}^{m} P(i)$. If ξ is a random number uniformly distributed in the range (0,1], an event m is selected according to

$$C(m-1) < \xi \leq C(m). \tag{6}$$

Once an event is selected, the system is changed correspondingly, the list of events updated, and the sequence repeated. To include time into the simulation, one needs to relate the probability of an event and its elapsed time. The reciprocal of the atomic jump frequency is a residence time for a defect cluster. Therefore, the residence time that would have elapsed for the system in a specific configuration is the reciprocal of the overall jump rate $\tau_r = 1/\sum_{i=1}^{M} r_i$. For random uncorrelated events, the distribution of event times is exponential if the process is Poissonian. Let ξ_2 be a random number in the range (0,1], then the elapsed time for a particular transition is given by [30]

$$\Delta t = -\tau_r \ln \xi_2. \tag{7}$$

A brief outline of the computational procedure is given below:

(1) introduce one single collision cascade into the simulation box;
(2) generate a sequence of jump frequencies for all possible events (equation (4));
(3) select an SIA cluster to execute a jump (equation (6));
(4) perform the jump and consider possible absorption and coalescence according to relative positions;
(5) update and sum up jump rates;
(6) advance the simulation clock by equation (7);
(7) iterate steps 1 through 6 until a specified damage dose is reached.

For an undisturbed crystal, the mean free path (MFP) until rotation in Fe for a 2-interstitial cluster is $\approx$8 jumps, for a 4-interstitial cluster it is $\approx$330 lattice jumps, and for a 6-SIAs it is 15 565 jumps, while the simulation box width is 400 lattice constants. However, simulation errors as a result of the MFP being larger than the box size are insignificant because of two aspects. (1) For a large-size cluster, using periodic boundary conditions enables continuation of the 1D motion until a rare event of thermally-induced rotation is encountered within the simulation box. This condition applies to the undisturbed crystal. (2) As the crystal fills up with defects, rotation of clusters is induced by their mutual interaction, or by chance encounter with dislocations. Thus, their MFP to rotation is effectively a few lattice jumps.

3.2. *Model assumptions and features*

The formation of a $\langle 100 \rangle$ interstitial loop by the interaction between two $1/2\langle 111 \rangle$ loops in bcc iron has been confirmed by both experiments [31] and for specific sizes, by MD simulations [32]. Experiments indicate that the process is more feasible at high temperature and larger irradiation dose [31]. In addition, Osetsky *et al*. [33] showed that SIA clusters containing a few $1/2\langle 111 \rangle$ crowdions are stable, and do not always join to form $\langle 100 \rangle$ interstitial loops. Since we consider low damage dose and room temperature irradiation, with SIA clusters directly emanating from cascades, the present investigation will focus on $\langle 111 \rangle$ interstitial loops, and thus the formation of $\langle 100 \rangle$ loops is not considered. The experimental observations of [18] indicate that

most SIA clusters are glissile, and hence may not be of the ⟨100⟩-type. We also exclude absorption reactions between grown-in dislocations and SIA clusters, since our major concern here is the segregation and agglomeration of defect clusters. Except for a direct encounter between a glissile loop and a dislocation, absorption of a loop by the dislocation requires a change in the direction of motion of the loop, either by a thermally activated Burgers vector change or by self-climb. Using MD simulations, Rodney and Martin investigated the mechanisms of the absorption of small interstitial loops by an edge dislocation in fcc nickel [34, 35]. They showed that interstitial clusters may find their stable positions a few lattice planes away from the glide plane of the dislocation [34]. The exclusion of absorption of interstitial loops by grown-in dislocations in the present work would not qualitatively affect the results of the present simulations, but would tend to overestimate the density of SIA clusters present at a given dose, as will be discussed in the next section.

As the cluster size increases, thermally-activated reorientation from one Burgers vector to another becomes increasingly more difficult and 3D motion of clusters is not observed even at very high temperatures. The activation energy for rotation has been estimated as 0.1 eV per SIA in a cluster (i.e. 0.4 eV for a 4-atom cluster [5]). Soneda and de la Rubia Diaz [6] studied the direction change frequency of 2-SIA and 3-SIA clusters in α-Fe using MD simulations and obtained the activation energies of 0.09 eV and 0.27 eV for 2-SIA and 3-SIA clusters, respectively. However, Gao *et al.* [36] investigated possible transition states of interstitials and small interstitial clusters in SiC and α-Fe using the dimer method, and found activation energies of 0.16, 0.09 and 0.54 eV for 1-, 2- and 3-SIA clusters in Fe, respectively, which are clearly larger than the values of [6]. The motion of small SIA clusters is the result of collective individual crowdion jumps [2, 7], and the reorientation may occur in a one-by-one fashion [33]. We therefore assume in the present work a linear relationship between the activation energy for directional change and the size of the cluster, with a slope of 0.05 eV per interstitial atom. This value is probably an underestimation for the energy barrier for direction change for small clusters (e.g. less than four), but would result in preferential 1D motion of a larger one.

Osetsky *et al.* [7] developed a generalized size dependence of cluster jump frequency to describe the one-dimensional diffusional transport behaviour of SIA clusters.

$$\omega^n = \omega_0 n^{-S} \exp\left(-\frac{E_m}{k_B T}\right), \tag{8}$$

where E_m is the average effective activation energy for migration, n is the number of SIAs in the cluster and ω_0 is a size-independent pre-exponential factor. The value of E_m was found not to depend on cluster size and to be close to that for an individual crowdion. For clusters containing up to 91 SIAs in iron $E_m = 0.023 \pm 0.003$ eV [7]. The values $\omega_0 = 6.1 \times 10^{12}\ s^{-1}$, $s = 0.66$ were found to describe the MD data for Fe [7].

In this section, we reveal some features of the KMC model by selecting size-independent activation energies and pre-factors for cluster motion for the purpose of performing *computational experiments* on collective cluster behaviour.

In the next section, however, the size dependence of these parameters [7] will be used to correlate with the experimental conditions of neutron-irradiated Fe.

A computational cell of $400\,a \times 400\,a \times 400\,a$ ($a = 0.2867$ nm is the lattice constant) is used with periodic boundary conditions. A fixed initial number of SIA clusters with the same size, $R = 3a$, is introduced randomly in the simulation box at 300 K. Their initial jump directions are also selected randomly. The initial SIA cluster number is varied, such that the density is in the range $5 \times 10^{22} - 2 \times 10^{23}\,\mathrm{m}^{-3}$. Size-independent parameters are used here. The value of the migration energy for these clusters is assumed to be 0.02 eV [7], with a pre-factor of $2.5 \times 10^{13}\,\mathrm{s}^{-1}$ and a value of $s = 0$. The activation energy for Burgers vector rotation is assumed to be 0.16 eV. A grown-in dislocation loop lying on the (101) plane, with Burgers vector $\mathbf{b} = a/2[\bar{1}11]$ is introduced into the simulation box. The dislocation loop consists of two curved segments and two straight super-jog segments that are normal to the loop's Burgers vector. The single dislocation loop corresponds to a dislocation density of $1.5 \times 10^{14}\,\mathrm{m}^{-2}$. The elastic constants are those for Fe ($\mu = 81.8$ GPa and $\nu = 0.29$). When a cluster approaches the dislocation loop within several lattice constants, it oscillates back and forth due to its strong interaction with the dislocation. To improve the computational efficiency of such fast dynamics, we used an *adiabatic approximation* by freezing trajectories of SIA clusters if a prescribed displacement is smaller than 1 nm over 10^4 time steps. Once a cluster is stopped, all events related to it are removed from the event table. When two SIA clusters approach one another within one atomic distance, they coalesce and form a larger one.

3.2.1. Dislocation decoration. Cluster–cluster interactions will first be excluded to gain insight into the influence of the elastic field of dislocations on the motion of SIA clusters. As can be seen in figure 1, the overall mobility and spatial distribution of SIA clusters were significantly changed as a result of dislocation–cluster interactions. After 0.4 ns, the majority of initially glissile clusters were attracted to the slip dislocation loop (near the edge components) and became virtually immobile. In effect, these clusters re-oriented themselves by rotation of their Burgers vectors to respond to the elastic field of dislocations. Thus, their migration was forced towards the source of the internal stress field, rather than being random. The high concentration of SIA clusters results in an extremely inhomogeneous spatial distribution, as can be seen in figure 1. For the same initial configuration as shown in figure 1a we also carried out KMC simulations without involving any interaction between SIA clusters and the slip dislocation loop. Figure 2 shows the final structure after running the same number of time steps as in figure 1. Even with introducing a standoff distance (taken as 1.5 nm) along the slip dislocation loop, there is no sign of development of dislocation decoration.

Comparison between figures 1d and 2 reveals that the elastic interaction significantly changes the kinetics of SIA clusters and thereby microstructure evolution. SIA clusters end up near the core of grown-in dislocations, orienting their Burgers vector parallel to the grown-in dislocation. They form a cluster atmosphere around the grown-in dislocation, similar to the Cottrell impurity atmosphere in bcc metals [16]. The present computer experiments show clearly how SIA clusters are attracted

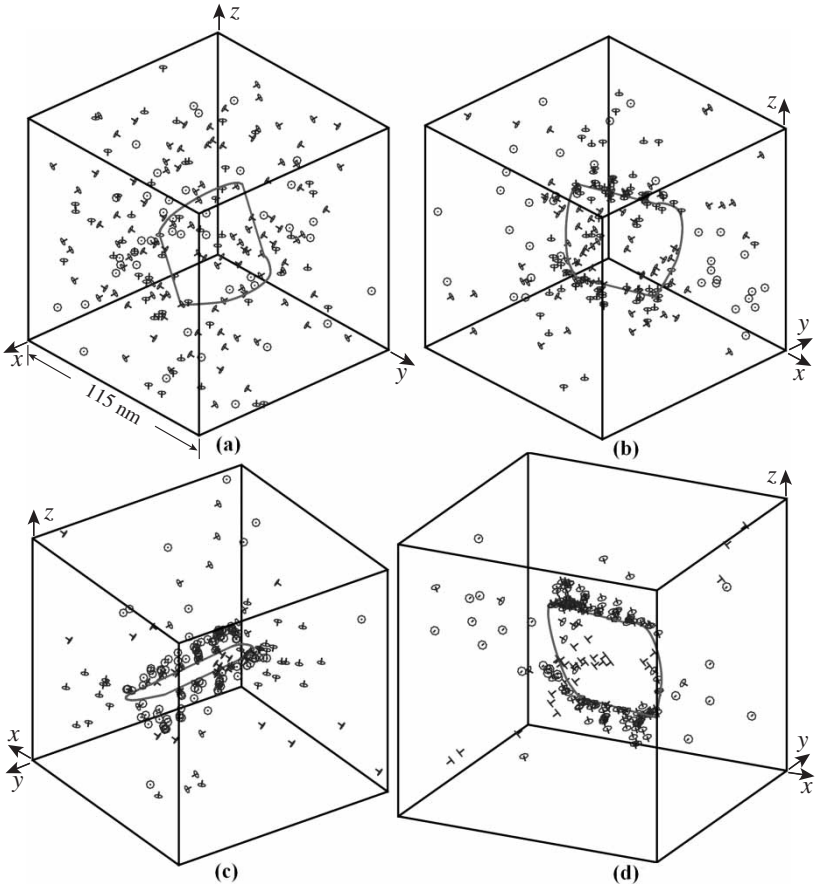

Figure 1. KMC simulation results of 200 SIA clusters in the stress field of a 3D dislocation loop, with interaction only between clusters and the dislocation. The dislocation $\mathbf{b} = [\bar{1}11]$ direction and the temperature is 300 K. SIA clusters are clearly observed to accumulate along the edge components of the loop. (a) 0 ns; (b) 0.1 ns; (3) 0.3 ns; (d) 0.4 ns.

to dislocations, eventually decorating them, in good qualitative agreement with experimental observations.

3.2.2. Pinning and small rafts. To investigate the effects of cluster–cluster interactions on their motion, the grown-in dislocation was removed and the elastic interaction between clusters included in a new KMC simulation. Mutual elastic interactions in between clusters was found to affect their distribution and motion drastically. Because of mutual interaction, two clusters that are oriented along non-parallel crystallographic orientations will either coalesce forming a larger one, or rotate and pin one another at a short distance and move jointly in the same direction. Once two clusters are pinned together, they have less chance to change their orientation, and therefore their motion becomes almost pure one-dimensional. As this process proceeds, some additional clusters may be trapped into this pinned

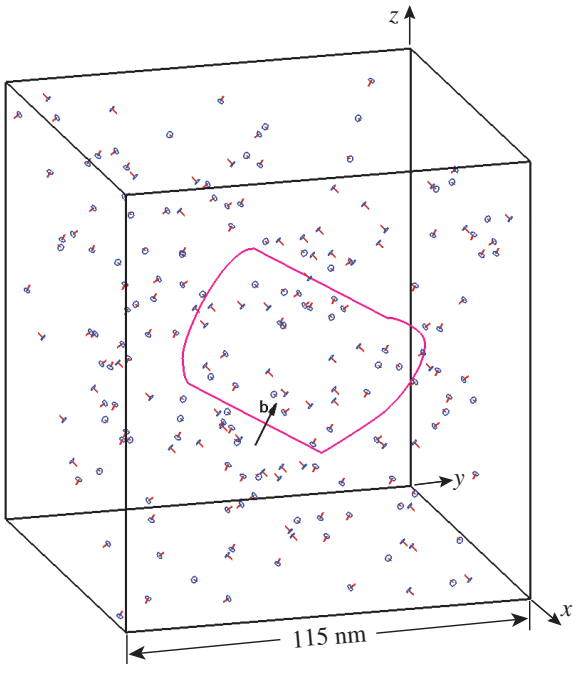

Figure 2. KKMC simulation results of 200 SIA clusters excluding all elastic interactions; otherwise conditions are the same as in figure 1. Dislocation decoration is not observed.

structure by changing their Burgers vectors. This self-organizing mechanism eventually results in the formation of SIA *rafts* , which consist of small dislocation loops with the same direction of motion. This feature has been experimentally observed for some time [16].

Another simulation of cluster motion including the influence of the internal stress field created by grown-in dislocations, as well as the clusters themselves was also performed. Figure 3 shows a typical defect evolution time sequence for 200 SIA clusters at 300 K. The effects of internal dislocation fields, aided by cluster mutual elastic interactions, rendered most of the clusters virtually immobile in the vicinity of the slip dislocation. Continuation of the decoration process results in the initiation of a 'dislocation wall'. Similar simulations were performed for a smaller cluster density (50 SIA clusters), and also at a higher temperature (600 K). At high temperatures, the kinetics of dislocation decorations is faster as a result of increased cluster jump rates. The simulations show that the *rafting* structure occurs more readily at lower temperatures. Decoration of dislocations with small clusters may require that trapped loops are immobilized by other loops to form a cluster atmosphere [16]. This concept is confirmed in figures 1 and 3, where the build-up of SIA cluster concentrations in the neighbourhood of the dislocation is clearly shown. As the decoration and loop raft formation processes proceed, the probability of interstitial clusters approaching dislocation cores decreases due to the screening effects of existing loops.

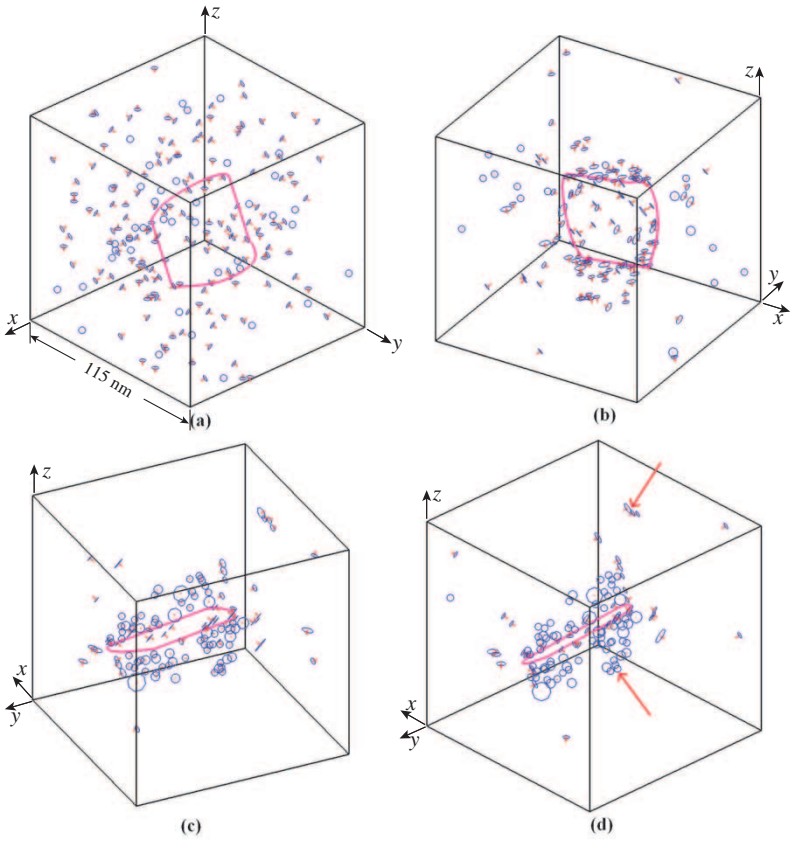

Figure 3. KMC simulation of 200 SIA clusters including elastic interactions in between clusters, and between clusters and the dislocation. Conditions are the same as in figure 1. Dislocation decoration and SIA cluster rafts are clearly observed, as indicated by the arrows. (a) 0 ns; (b) 0.4 ns; (3) 0.7 ns; (d) 1.0 ns.

4. Comparison with experiments on neutron-irradiated iron

In this section, we perform KMC computer simulations for the microstructure evolution of pure Fe irradiated at $\simeq 70^{\circ}$C in the HFIR reactor to displacement dose in the range of $(0.0001 - 0.72)$ dpa [18], and for pure iron irradiated in the DR-3 reactor at RISØ National Laboratory at 320 K [37]. One of the most striking features in the evolution of dislocation microstructure under cascade damage conditions is that most dislocations are observed to be heavily decorated by small, immobilized interstitial clusters. Rafts of small defect clusters are clearly observed in neutron-irradiated pure iron [18, 38].

4.1. *Irradiation conditions and parameters*

Fitting MD-generated data for several metals, Bacon *et al.* [2] showed that the number of Frenkel pairs in a cascade (N_{F}) is given by $N_{\mathrm{F}} = A(E_{\mathrm{PKA}})^{m}$, where

A and m are constants and E_{PKA} is the energy of the Primary Knock On Atom. On the other hand, the number of displaced atoms can be written as $N_F = PN_t$, where P is the displacement dose (dpa) and N_t is the total number of atoms in the system. Therefore, the displacement dose corresponding to one cascade can be readily calculated as

$$P = \frac{N_F}{N_t} = \frac{A(E_{PKA})^m}{N_t}. \tag{9}$$

Equation (9) was used to determine the number and frequency of cascades required for producing a desired dose at a given dose rate. Point defect statistics for clusters generated by 40 keV cascades in α-Fe (e.g. number, size distribution, and mobility) were taken from the MD simulations of [2]. Soneda and de la Rubia Diaz [6] have shown that two thirds of the defects that escape from the parent cascade region are in the form of small SIA clusters, which migrate in one dimension. Therefore, mono-defects as well as relatively smaller clusters were ignored in the present simulations. Room temperature neutron irradiation of iron was simulated with a flux of 40 keV cascades containing interstitial clusters of size $\geq$4 atoms.

MD simulations revealed that the defect structure of a cascade is characterized by a vacancy-rich core surrounded by a shell of SIA clusters. We represent this vacancy-rich core region here as an immobile spherical recombination centre. The size of a recombination centre (or nano-void) is given by an equivalent diameter. The number of vacancies in the core of a cascade is assumed to follow a Gaussian distribution with a mean value of 100 and a standard deviation of 8 vacancies.

4.2. *Dose dependence of defect density*

It is instructive to compare the predictions of the present model (with the assumptions stated above) to the experimental results of Singh *et al.* [37] and Eldrup *et al.* [18] on neutron-irradiated iron. For the same experimental conditions, displacement damage doses up to 5.2×10^{-3} dpa were simulated at a rate of 5×10^{-8} dpa s^{-1}. Figure 4 shows the interstitial cluster density as a function of dose, with and without recombination between SIA clusters and nano-voids. At low dose ($<10^{-4}$ dpa), the cluster density increases almost linearly with dose. The increase in cluster density then slows down when the dose is higher than 10^{-4} dpa, and does not change much beyond 3.5×10^{-3} dpa. The presence of nano-voids has a significant effect on the evolution dynamics of SIA clusters. At a dose lower than 5×10^{-4} dpa, the difference between SIA cluster density, with and without nano-voids, is not large, as can be seen in figure 4. However, the density of surviving SIA clusters is reduced by a factor of 2 at 1.5×10^{-3} dpa, when nano-voids are included.

Experimental observations of small defect clusters depend on the minimum size that can be resolved. A value between 1.5 and 2 nm in diameter is quoted in the literature as the minimum size resolved by TEM [39]. Considering SIA clusters containing more than 100 interstitial atoms (diameter >2.5 nm) as *visible* defects, a comparison between the present model and experiments is shown in figure 5. At the beginning of irradiation, cluster densities of both interstitials and vacancies are rather low and the chance that one interstitial cluster can get close enough to another interstitial or vacancy cluster is small. Because of the 1D motion of

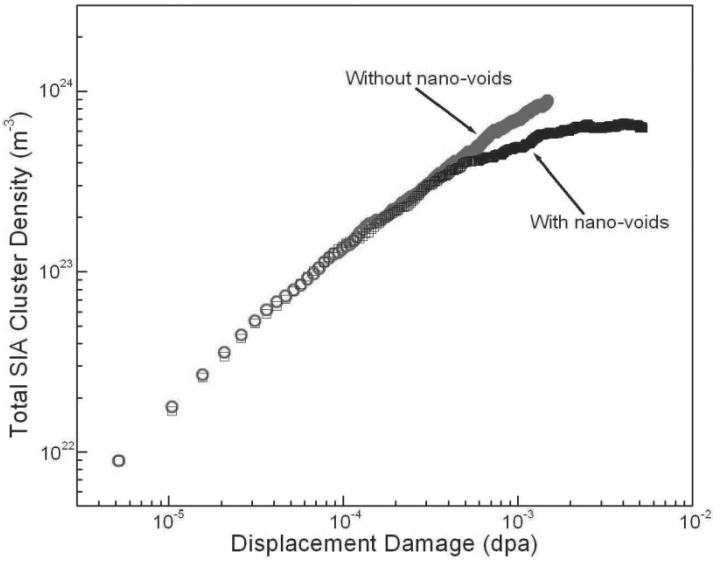

Figure 4. Dose dependence of the total SIA cluster density in bcc Fe: -◯-, no recombination; -□- with recombination.

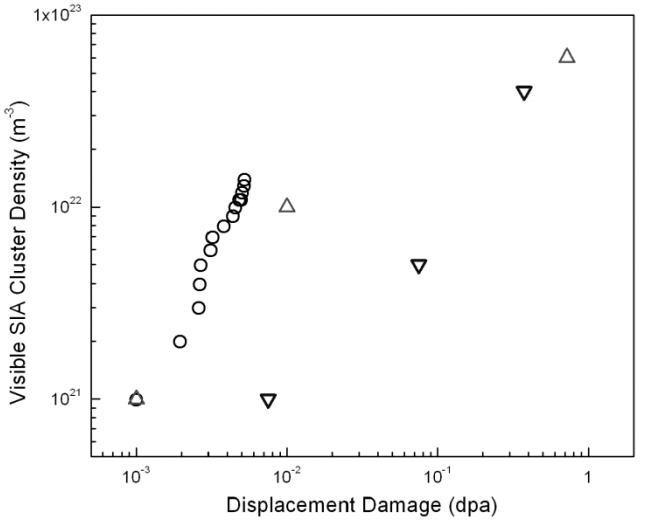

Figure 5. Dose dependence of the total visible SIA cluster density in bcc Fe: -◯-, KMC simulation results; -△- experimental results of Eldrup *et al.* [18]; -▽- experimental results of Singh *et al.* [37].

SIA clusters, the recombination rate with nano-voids and the coalescence rate with other interstitial clusters are small. Thus the density of clusters increases almost linearly with dose. When the damage builds up to an appreciable level, on the order of 10^{-4} dpa, the simulation box becomes crowded with defects. The probability

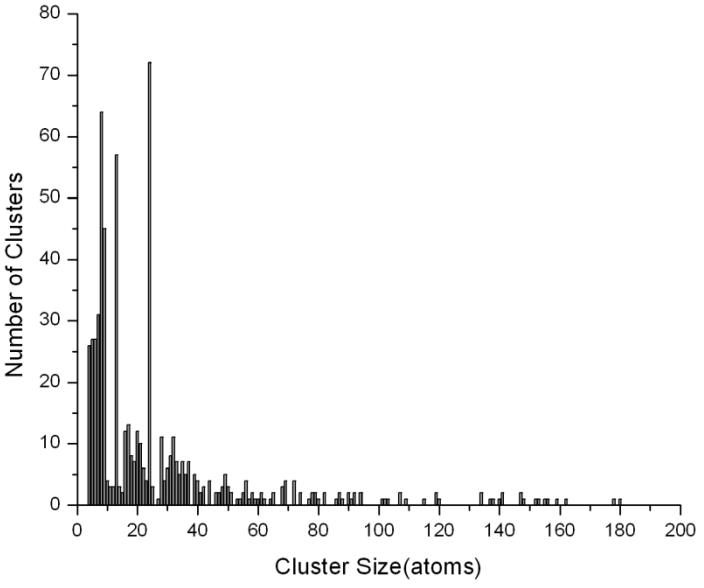

Figure 6. Size distribution of SIA clusters at a dose level of 5.21×10^{-3} dpa.

of mutual interaction between clusters becomes appreciable, leading to more pronounced recombination and coalescence events. Consequently, these nonlinear reactions slow down the increase in the density of SIA clusters. At higher dose, on the order of 3.5×10^{-3} dpa, the number of SIA clusters that recombine or coalesce reaches dynamic equilibrium with the number of clusters produced by fresh cascades. The SIA cluster density in the simulation box reaches an equilibrium level.

Although the density of SIA clusters reaches steady state at about 3.5×10^{-3} dpa, SIA cluster sizes continue to grow and the density of visible clusters increases as well. It is shown in figure 5 that the density of visible SIA clusters obtained in the simulations presented here is larger than the experimental measurement at high dose levels. The high mobility of SIA clusters allows them to be absorbed on other sinks, such as grain boundaries or free surfaces. Hence we can consider the agreement with the experimental conditions on the cluster density [18] as qualitative.

The size distribution of SIA clusters at a dose of 5.2×10^{-3} dpa is shown in figure 6. More than half the interstitial clusters consist of more than 30 defects, though small clusters consisting of less than 10 SIAs still have the largest concentration. It can be expected that the size distribution will continue to shift to larger sizes as damage accumulates. It is found here that a mobile SIA cluster can be immobilized, either by getting trapped near a dislocation or by getting locked with another large cluster (>37 SIAs) of a different Burgers vector.

4.3. *Characteristics of decoration and raft formation*

The dislocation decoration process builds up quickly with dose, and already at 3×10^{-4} dpa, grown-in dislocations begin to attract SIA clusters. At higher dose,

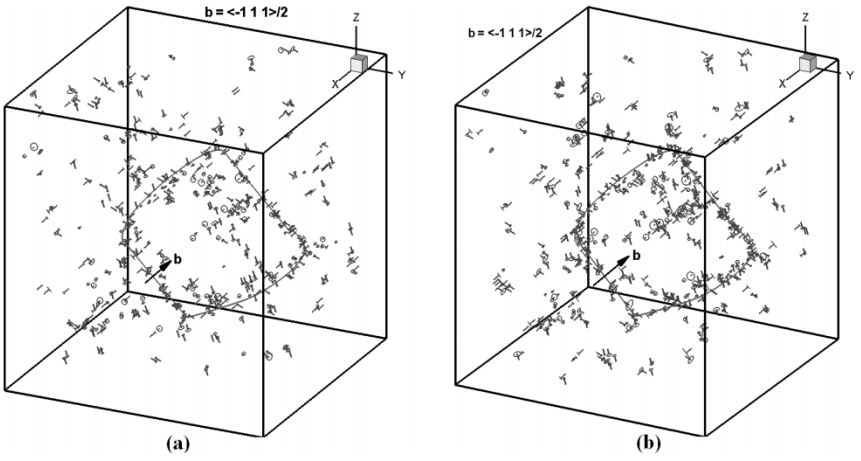

Figure 7. Spatial distribution of SIA clusters in bcc Fe at 300 K, (a) 1.3×10^{-3} dpa, (b) 5.2×10^{-3} dpa.

dislocation decoration becomes very significant, as can be seen in figure 7. When an extremely mobile 1D migrating interstitial cluster passes through the neighbourhood of a pre-existing dislocation, it will feel the influence of its strain field. As long as the defect-dislocation interaction is attractive and the distance is small, the cluster cannot escape from the attractive zone by thermally-activated random walk. Once a SIA cluster is permanently trapped into the strain field of a dislocation, the decoration of the grown-in dislocation begins [16, 40].

It can be clearly seen in figure 7b that the pure edge components of the slip dislocation attract more SIA clusters in its vicinity. Trapped clusters can still serve as sinks for the glissile clusters and increase their size before they rotate their Burgers vectors and finally get absorbed by dislocations. With the accumulation of clusters along the dislocation line, a repulsive force field is then gradually built up against further cluster trapping. Figure 8a shows contours of the interaction energy between an interstitial defect cluster of Burgers vector $a/2[\bar{1}\ 1\ 1]$ and an edge dislocation on the $(\bar{1}\ \bar{2}\ 1)$-plane in bcc iron; and figure 8b shows contours of the interaction energy between an interstitial defect cluster of Burgers vector $a/2[\bar{1}\ 1\ 1]$ and a pre-existing same type cluster and an edge dislocation on the $(\bar{1}\ \bar{2}\ 1)$-plane.

When the attractive stress field of the dislocation is fully compensated for by existing clusters, the SIA content in the primary trapping region achieves saturation and the decoration process stops. Although dislocation decoration saturates at a low dose, the primary region of cluster trapping shifts the stress field of the dislocation and cluster trapping occurs only ahead of the existing dislocation/loop structure, where the interaction remains attractive [16]. For increasing dose, cluster trapping continues away from the dislocation and results in dislocation wall formation. As seen in figure 3d, the present simulations show the extension of cluster trapping and the formation of a dislocation wall.

In addition to dislocation decoration, another major striking feature of microstructure evolution is the formation of dislocation loop rafts. Figure 9 shows

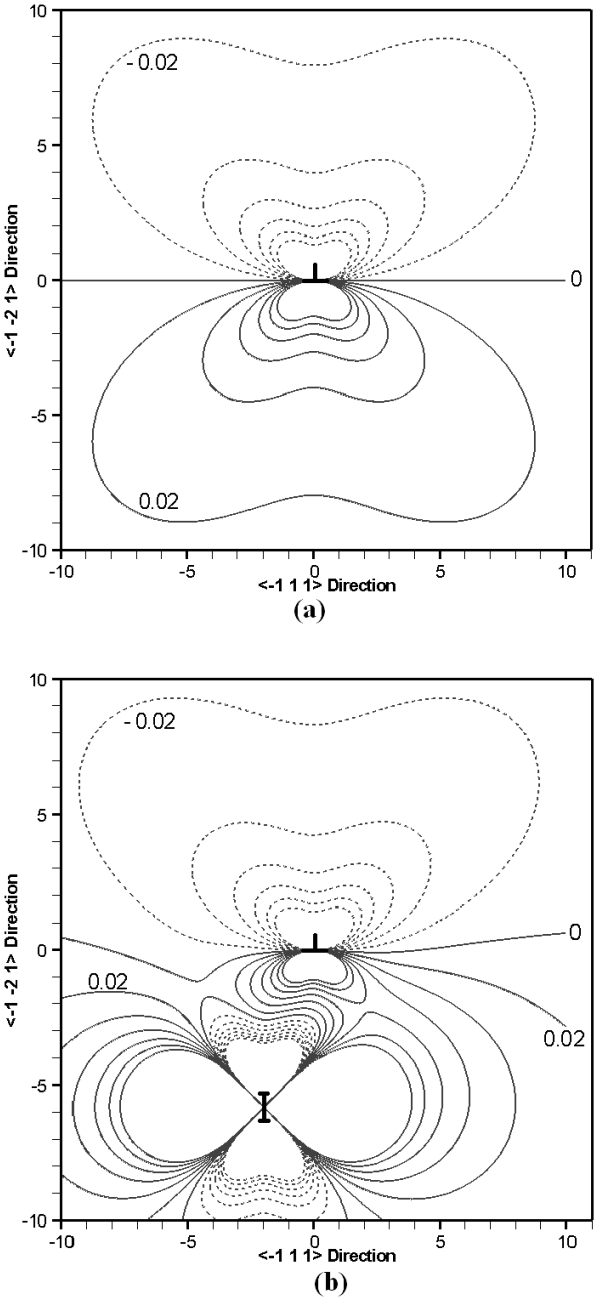

Figure 8. (a) Local iso-energy contours for the interaction energy of a SIA cluster of Burgers vector $a/2[\bar{1}11]$ with an edge dislocation on the $(\bar{1}\bar{2}1)$-plane in bcc iron; (b) local iso-energy contours of the interaction energy of an interstitial defect cluster of Burgers vector $a/2[\bar{1}11]$ with a pre-existing same type cluster and an edge dislocation on the $(\bar{1}\bar{2}1)$-plane. Contours are plotted at 0.02 (in $\mu\delta A/(1-\nu)$, where μ is the shear modulus and δA is the surface area of the SIA cluster) increment. The length on the axes is in units of lattice constant, a.

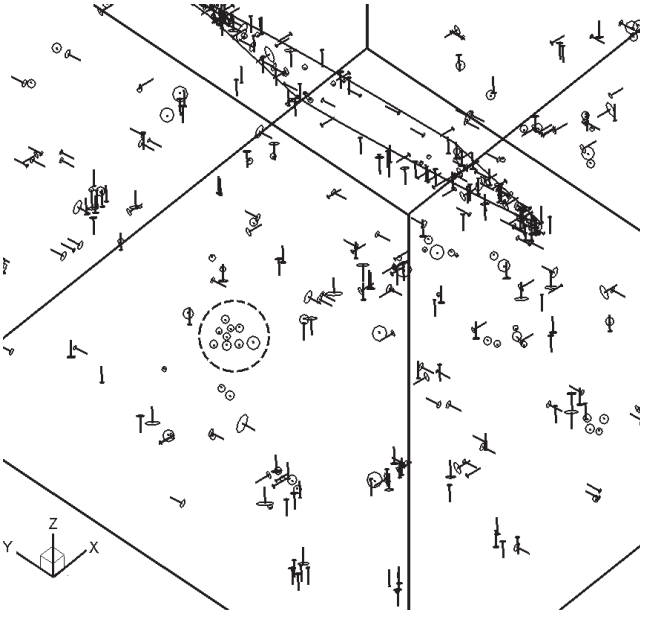

Figure 9. A close-up view of the configuration of a raft of interstitial clusters formed at a dose level of 1.8×10^{-3} dpa. The raft is enclosed in a dotted circle.

a configuration of SIA cluster raft formed at a dose level of 1.8×10^{-3} dpa. The Burgers vectors of the clusters making up the raft are all parallel to one another, which is in agreement with experimental observations [16]. If the interaction between two close SIA clusters is attractive and strong enough to overcome the energy barrier for directional change, they adjust their relative positions and orientations. This scenario is similar to the pinning of clusters, which has been demonstrated in the previous section.

To shed light on the nature of cluster–cluster self-trapping, we consider the forces between two identical clusters. In figure 10, a prismatic dislocation loop is fixed at the origin and another identical one is moved along its slip direction. The glide force on the moving loop is plotted as a function of its relative position. It is shown that 5 equilibrium positions (zero force) exist between the two parallel clusters. However, only two of them are stable, at a relative angle of $\pm 70.1^{\circ}$. When multiple clusters interact, this simple picture is somewhat disturbed. Nevertheless, extended stable cluster complexes form by this self-trapping mechanism. Figure 11 shows the force field along the slip direction of an existing raft obtained in our simulations. Two additional clusters that will join the raft in the following time step are also shown with dotted lines. It can be seen that raft formation is *autocatalytic*, since a raft nucleus is stable, but keeps expanding through the association of other clusters on its periphery. As the number of clusters within a raft increases, the mobility of the raft as a whole decreases. The decrease in the mobility of individual clusters can be attributed to mutual elastic interactions between clusters that are members of a raft.

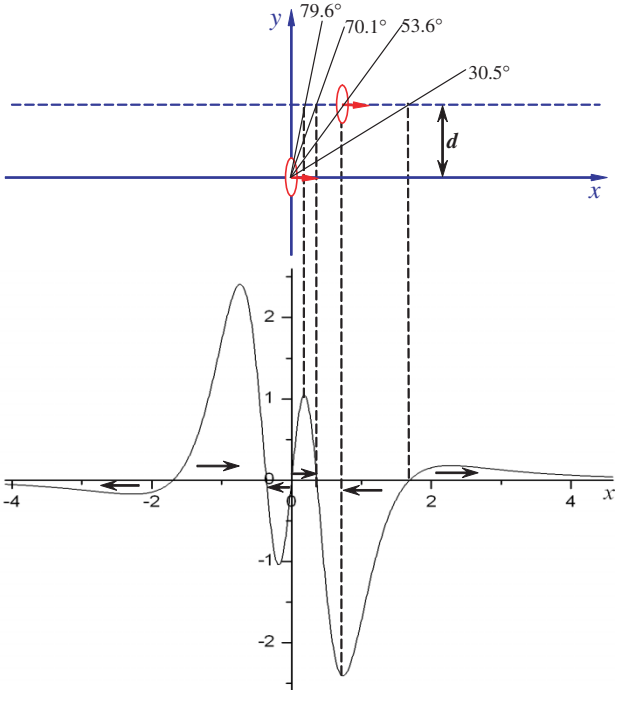

Figure 10. The glide force between two prismatic dislocation loops with parallel Burgers vectors as a function of their relative positions. The force is scaled by $\mu b_1 b_2 A_1 A_2 / 4\pi(1-\nu)d^4$, where b_i and A_i $(i = 1, 2)$ are the Burgers vectors and surface areas of the two loops, respectively.

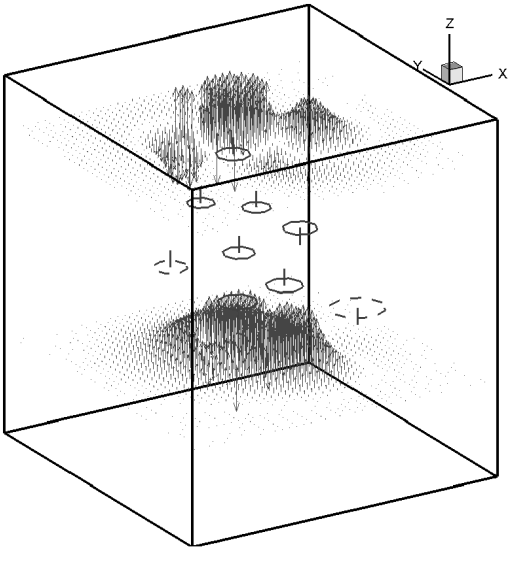

Figure 11. Force field distribution along the glide direction of an existing raft of SIA clusters (in solid lines). Two new SIA clusters (in dashed line) which will join the raft are also shown.

4.4. *Conditions for decoration and raft formation*

Trinkaus *et al.* [16] have shown that a grown-in dislocation would have a large drainage area for accumulating one-dimensionally migrating glissile loops in its neighbourhood. Our simulations also demonstrate that even at a fairly low dose of 1.3×10^{-3} dpa, clear dislocation decoration is observed. The energy barrier for directional change is a critical parameter in controlling when, how and to what extent dislocation decoration and raft formation occur. The maximum range for the elastic interaction that is strong enough to overcome the barrier and thereby leads to a Burgers vector change is strongly dependent on this parameter. In other words, the interaction between defects and the microstructure contributes to dislocation decoration and the formation of rafts in terms of changing the diffusivity and the characteristics of mixed 1D/3D migration. Brimhall and Mastel [9] proposed that loops move through the lattice by a combination of prismatic glide and self-climb to form rafts. Our present simulations, however, suggest that raft formation could be achieved just by prismatic glide and rotation of glissile SIA clusters. A necessary condition for pronounced formation of rafts is that the group of clusters within a raft is large enough to trap a single glissile cluster in the strain field formed by the group and prevent it from further Burgers vector rotation. Our simulations indicate that small rafts containing two or three clusters are still mobile; more specifically, these small patches still perform 1D migration, although at reduced mobility. With the size of a patch increasing, the overall mobility decreases, and a raft consisting of more than five clusters is literally immobile. Due to thermal activation or interaction with other defects, a SIA cluster trapped in the outer region of a raft may break away and detrap from the raft.

5. Conclusions

An approach for KMC simulations that incorporates the continuous generation of point defect clusters and the elastic interaction between various components of the microstructure has been developed. The model has been applied to the investigation of point defect segregation and damage accumulation under cascade irradiation in bcc Fe. The following features are in qualitative agreement with experimental observations: (1) the overall sessile SIA cluster density and its dose dependence, (2) the formation of dislocation decoration and (3) the autocatalytic formation of SIA cluster rafts and their Burgers vector orientation. Furthermore, the fact that the rafts are experimentally observed is consistent with our finding of their overall low mobility.

Glissile SIA clusters produced in displacement cascades have been demonstrated to play a decisive role in the evolution of a spatially heterogeneous microstructure. The 1D motion of glissile SIA clusters and the interaction between defects and the dislocation microstructure were shown to be the main cause for the appearance and development of decorations and rafts. At rather low dose around 1.0×10^{-3} dpa, a large portion of the initially glissile clusters are shown to be trapped around grown-in dislocation loops (the majority of them are distributed near the edge component) and become virtually immobile. The high concentration of SIA loops around grown-in dislocations results in an inhomogeneous spatial distribution. The simulations

shed light on the physics of raft formation and dislocation decoration during irradiation of bcc metals. The present work suggests that raft formation can be achieved by prismatic glide of glissile interstitial clusters and rotation of their Burgers vectors under the influence of internal strain fields (e.g. generated by dislocations).

Acknowledgments

The present work was supported by the US Department of Energy (DOE), Office of Fusion Energy Sciences (OFES) through grant DE-FG02-03ER54708 with UCLA, and partly funded by the European Fusion Technology Programme.

References

[1] B. von Guerard, D. Grasse and J. Peisl, Phys. Rev. Lett. **44** 262 (1980).
[2] D.J. Bacon, F. Gao and Y.N. Osetsky, J. Nucl. Mater. **276** 1 (2000).
[3] A.F. Calder and D.J. Bacon, J. Nucl. Mater. **207** 25 (1993).
[4] T. Diaz de la Rubia and M.W. Guinan, Phys. Rev. Lett. **66** 2766 (1991).
[5] A.J.E. Foreman, C.A. English and W.J. Phythian, Phil. Mag. A **66**(5) 655 and 671 (1992).
[6] N. Soneda and de la Rubia Diaz, Phil. Mag. A **78** 995 (1998).
[7] Y.N. Osetsky, D.J. Bacon, A. Serra, *et al.*, J. Nucl. Mater. **276** 65 (2000).
[8] N. Soneda and de la Rubia Diaz, Phil. Mag. A **81** 331 (2001).
[9] J.L. Brimhall and B. Mastel, Radiat. Effects **3** 203 (1970).
[10] A.J.E. Foreman and J.D. Eshelby, Technical Report R4170 (Atomic Energy Research Establishment, Harwell, UK, 1962).
[11] R.S. Barnes, J. Phys. Soc. Japan Suppl. III **18** 305 (1963).
[12] G.P. Seidel, Radiat. Effects **1** 177 (1969).
[13] B.N. Singh, A.J.E. Foreman and H. Trinkaus, J. Nucl. Mater. **249** 103 (1997).
[14] J. Huang and N.M. Ghoniem, J. Comput. Mater. Sci. **23** 225 (2002).
[15] F. Kroupa, in *Theory of Crystal Defects*, edited by B. Gruber (Academic Press, New York, 1966), p. 275.
[16] H. Trinkaus, B.N. Singh and A.J.E. Foreman, J. Nucl. Mater. **249** 91 (1997).
[17] B.L. Eyre, D.M. Maher and A.F. Bartlett, Phil. Mag. A **24** 767 (1971).
[18] M. Eldrup, B.N. Singh, S.J. Zinkle, *et al.*, J. Nucl. Mater. **307–311** 912 (2002).
[19] J.H. Evans, J. Nucl. Mater. **88** 31 (1980).
[20] V.K. Sikka and J. Moteff, J. Nucl. Mater. **54** 325 (1974).
[21] B.N. Singh, J.H. Evans, A. Horsewell, *et al.*, J. Nucl. Mater. **258–263** 865 (1998).
[22] K. Yamakawa and Y. Shimomura, J. Nucl. Mater. **155–157** 1211 (1988).
[23] A.H. Cottrell, *Dislocations and Plastic Flow in Crystals* (Oxford University Press, London, 1953).
[24] Y. Satoh, I. Ishida, T. Yoshiie, *et al.*, J. Nucl. Mater. **155–157** 443 (1988).
[25] H.L. Heinisch and B.N. Singh, J. Nucl. Mater. **271–272** 46 (1999).
[26] R. Bullough and J.R. Hardy, Phil. Mag. **17** 833 (1968).
[27] R. Siems, Phys. Status Solidi **30** 645 (1968).
[28] N.M. Ghoniem and L.Z. Sun, Phys. Rev. B **60** 128 (1999).
[29] N.M. Ghoniem, Trans. ASME, J. Eng. Mater. Tech. **121** 136 (1999).
[30] A. Bortz, M.H. Kalos and J.L. Lebowitz, J. Comput. Phys. **17** 10 (1975).
[31] E.A. Little, R. Bullogh and M.H. Wood, Proc. R. Soc. A **372** 565 (1980).
[32] J. Marian, B.D. Wirth and J.M. Perlado, Phys. Rev. Lett. **88** 255507 (2002).
[33] Y.N. Osetsky, A. Serra and V. Priego, J. Nucl. Mater. **276** 202 (2000).
[34] D. Rodney and G. Martin, Phys. Rev. Lett. **82** 3272 (1999).
[35] D. Rodney and G. Martin, Phys. Rev. B **61** 8714 (2000).

[36] F. Gao, G. Henkelman, W.L. Weber, *et al.*, Nucl. Instr. Meth. B **202** 1 (2003).
[37] B.N. Singh, A. Horsewell and P. Toft, J. Nucl. Mater. **271–272** 97 (1999).
[38] B.N. Singh, RISO Report RISO-R-1422[EN] (Roskilde, Denmark, 2003).
[39] B.N. Singh and S.J. Zinkle, J. Nucl. Mater. **206** 212 (1993).
[40] H. Trinkaus, B.N. Singh and A.J.E. Foreman, J. Nucl. Mater. **251** 172 (1997).